Extending the Numerical Stability Limit of Terrain-Following Coordinate Models over Steep Slopes

GÜNTHER ZÄNGL

Deutscher Wetterdienst, Offenbach, Germany

(Manuscript received 10 February 2012, in final form 27 April 2012)

ABSTRACT

To extend the numerical stability limit over steep slopes, a truly horizontal pressure-gradient discretization based on the ideas formulated by Mahrer in the 1980s has been developed. Conventionally, the pressure gradient is evaluated in the terrain-following coordinate system, which necessitates a metric correction term that is prone to numerical instability if the height difference between adjacent grid points is much larger than the vertical layer spacing. The alternative way pursued here is to reconstruct the pressure gradient at auxiliary points lying at the same height as the target point on which the velocity is defined. This is accomplished via a second-order Taylor-series expansion in this work, using the hydrostatic approximation to transform the second derivatives into first derivatives to facilitate second-order accurate discretization in the presence of strong vertical grid stretching. Moreover, a reformulated lower boundary condition is used that avoids the extrapolation of vertical derivatives evaluated in potentially very thin layers. A sequence of tests at varying degrees of idealization reveals that the truly horizontal pressure-gradient discretization improves numerical stability over steep slopes for a wide range of horizontal mesh sizes, ranging from a few hundreds of meters to tens of kilometers. In addition, tests initialized with an atmosphere at rest reveal that the spurious circulations developing over steep mountains are usually smaller than for the conventional discretization even in configurations for which the latter does not suffer from stability problems.

1. Introduction

Despite their well-known limitations in handling steep orography, the vast majority of the atmospheric models used for operational weather forecasting and research applications is based on terrain-following coordinates. This is primarily because height-based (Cartesian) coordinates impose other problems that are even more difficult to handle for general-purpose models. While the obvious errors of step coordinates in treating flow over mountains reported by Gallus and Klemp (2000) can be relatively easily avoided with approaches like cut cells (e.g., Steppeler et al. 2002), coupling with physics parameterizations remains difficult because, for example, currently available boundary layer parameterizations rely on a high and as uniform as possible vertical resolution near the surface. Therefore, efforts are still ongoing to further alleviate the disadvantages of terrain-following coordinates over steep terrain.

In this context, the most active research field in the last decade was probably the specification of the vertical coordinate. While the use of hybrid coordinates transitioning into pure height (or pressure) levels above a certain height (below a certain pressure) has been standard for a long time, Schär et al. (2002) proposed a generalized coordinate definition that allows for an even faster decay of the topography signal in the coordinate surfaces. For this so-called smooth-level vertical coordinate (SLEVE), the topography is first split into a heavily smoothed (large scale) part and a corresponding small-scale deviation. The coordinate is then set up by specifying vertical decay functions for the large-scale and small-scale parts, with the latter decaying much faster with height in order to minimize the discretization errors away from the topography. The SLEVE coordinate was then transferred from height-based (Gal–Chen) to pressure-based terrain-following coordinates by Zängl (2003). More recently, Leuenberger et al. (2010) presented a further generalization of the SLEVE coordinate that avoids the occurrence of very thin model layers over mountain peaks, which may induce numerical stability problems under unfavorable conditions. An even more

Corresponding author address: Günther Zängl, Deutscher Wetterdienst, Frankfurter Straße 135, D-63067 Offenbach, Germany.
E-mail: guenther.zaengl@dwd.de

DOI: 10.1175/MWR-D-12-00049.1

advanced method was proposed by Klemp (2011), based on a smoothing of the coordinate surfaces that progressively increases when moving away from the ground. In general, sophisticated coordinate definitions can greatly alleviate topography-related discretization errors at sufficient vertical distance from the ground, but there is naturally little improvement at low levels where the coordinate surfaces are still mostly aligned to the topography.

Probably the most critical discretization error is that of the horizontal pressure gradient term, which can induce spurious circulations over mountainous topography and even numerical instability if the mountains are steep enough. One of the first studies specifically analyzing pressure-gradient discretization errors was undertaken by Gary (1973), who concluded that the use of a perturbation pressure may help in reducing these errors. Using a perturbation pressure is nowadays standard in nonhydrostatic models. For hydrostatic models, a hydrostatically consistent vertical integration of the geopotential has been found to be important (e.g., Mesinger 1982), and Janjić (1989) reported that spectral models tend to suffer from larger pressure-gradient discretization errors over steep mountains than gridpoint models, partly because the errors are nonlocal in spectral models. For gridpoint models, Mahrer (1984) proposed a pressure-gradient discretization that starts with a reconstruction of the pressure at auxiliary points having the same height as the velocity point under consideration, and then takes a truly horizontal gradient without a metric correction term. Wherever possible without intersecting the topography, the reconstruction is a simple interpolation between the two adjacent model levels, which usually leads to smaller discretization errors than the standard discretization along terrain-following coordinates. A more detailed analysis of various interpolation methods was undertaken by Dempsey and Davis (1998), who concluded on the basis of atmosphere-at-rest tests that quadratic polynomial interpolation (including quadratic extrapolation to grid points lying below the ground) shows the best performance of the methods considered. For reasons one could only speculate about, Mahrer's approach never became widely used in atmospheric community models, but very recently, Klemp (2011) proposed a simplified version of Mahrer's discretization that still significantly reduces the discretization errors.

In this paper, an extension of Mahrer's ideas is presented that substantially increases the numerical stability over steep slopes by avoiding the extrapolation over a large distance of vertical pressure gradients that are calculated in the usually very thin lowest model layer. It is combined with a truly horizontal temperature diffusion similar to that described in Zängl (2002) but now implemented in a way that does not add significant computational cost. The derivation of the scheme and its numerical implementation are described in section 2. Results of a selection of idealized simulations are shown in section 3, followed by a summary of our findings in section 4.

2. Formulation of the scheme

a. Background: The dynamical core

The work presented here has been done in the frame of the development of the icosahedral nonhydrostatic (ICON) model, which is a joint effort of Deutscher Wetterdienst (DWD; the National Weather Service of Germany) and the German Max Planck Institute for Meteorology (MPI-M). ICON is a global model based on an icosahedral-triangular C grid with grid-nesting capability (one-way or two-way nesting) and can also be run in a limited-area mode. As the model documentation is still in preparation, some background information on the dynamical core and its numerical implementation is provided here. The basic equation system, omitting diabatic terms, reads as

$$\frac{\partial v_n}{\partial t} - (\zeta + f)v_t + \frac{\partial K}{\partial n} + w\frac{\partial v_n}{\partial z} = -c_{\mathrm{pd}}\theta_v\frac{\partial \pi}{\partial n}, \tag{1}$$

$$\frac{\partial w}{\partial t} + \nabla\cdot(\mathbf{v}_h w) - w\nabla\cdot\mathbf{v}_h + w\frac{\partial w}{\partial z} = -c_{\mathrm{pd}}\theta_v\frac{\partial \pi}{\partial z} - g, \tag{2}$$

$$\frac{\partial \rho}{\partial t} + \nabla\cdot(\mathbf{v}\rho) = 0, \tag{3}$$

$$\frac{\partial \rho\theta_v}{\partial t} + \nabla\cdot(\mathbf{v}\rho\theta_v) = 0. \tag{4}$$

The prognostic variables are the horizontal velocity component normal to the triangle edges v_n, the vertical wind component w, density ρ, and virtual potential temperature θ_v. The remaining symbols are the vertical vorticity component ζ, the Coriolis parameter f, the (reconstructed) tangential velocity component v_t, the horizontal part of the kinetic energy $K = 1/2(v_n^2 + v_t^2)$, the Exner function π, the specific heat capacity of dry air at constant pressure c_{pd}, and the gravitational acceleration g. Here $\partial/\partial n$ denotes a horizontal derivative in edge-normal direction (i.e., between the two adjacent mass points). The equations are solved with a two-time-level predictor-corrector scheme that is fully explicit in the horizontal and implicit for the terms describing vertical sound wave propagation. The dynamical core thus has to be integrated at the (horizontal) sound wave time step, but in the full model with physics coupling, a longer time step (usually 4× in global applications) is used for tracer advection and the fast-physics parameterizations. It is

mentioned that the vertically implicit acoustic solver applies off-centering in time by a user-selectable amount, which is primarily needed to prevent sound wave resonance in configurations with very high model tops, but also helps with stabilizing the dynamical core over steep slopes (Dudhia 1995). As vertical coordinate, a hybrid Gal–Chen coordinate and the generalized SLEVE coordinate described by Leuenberger et al. (2010) are available, complemented by a layer-thickness limiter that safely avoids too closely spaced (or even intersecting) model layers over high mountain peaks without any tuning effort on the coordinate parameters. For numerical stability, a weak fourth-order filter term (divergence damping or diffusion) is added to Eq. (1), but no artificial diffusion term is needed for the scalar quantities because advection of ρ and θ_v is discretized with an upwind-biased second-order accurate scheme following Miura (2007). The numerical diffusion can be combined with a second-order Smagorinsky diffusion for v_n and θ_v, which is usually evaluated along the terrain-following coordinate surfaces, but an option for a truly horizontal computation of θ_v diffusion is available as described below. In addition, an option for using a reference state for pressure gradient computation is available, but it is noted here that because the curvature of π is much smaller than that of pressure (for an isentropic atmosphere, $\partial\pi/\partial z$ is even a constant), the accuracy gain due to the reference state is relatively small in this case.

b. Discretization of the horizontal pressure gradient

In the equation system outlined above, the conventional pressure gradient discretization along terrain-following coordinates reads as

$$\left.\frac{\partial\pi}{\partial n}\right|_z = \left.\frac{\partial\pi}{\partial n}\right|_s - \left.\frac{\partial h}{\partial n}\right|_s \overline{\frac{\partial\pi}{\partial z}}, \tag{5}$$

where s denotes a terrain-following coordinate surface, h is the height of the grid points lying on it, and the overbar indicates a horizontal average from mass points to a velocity point. The basic idea of Mahrer (1984) was to replace this by

$$\left.\frac{\partial\pi}{\partial n}\right|_z = \frac{1}{d_{12}}(\pi_2^* - \pi_1^*), \tag{6}$$

where 1 and 2 denote the adjacent mass points, d_{12} is the distance between them, and π^* stands for a reconstructed (Exner) pressure at the height of the velocity point for which the gradient needs to be evaluated. The reconstruction of π^* can be accomplished through an interpolation between the adjacent model levels, or through a Taylor-series expansion starting from the mass point closest to the target height, as described in the following. In both cases, the model level indices between which the pressure reconstruction is executed need to be precomputed and stored, because in typical model applications, the height difference between neighboring grid points can greatly exceed the vertical layer spacing. Here we propose a second-order Taylor-series expansion:

$$\pi^* = \pi_{\mathrm{k1}} + \left.\frac{\partial\pi}{\partial z}\right|_{\mathrm{k1}} (h^* - h_{\mathrm{k1}}) + \frac{1}{2}\left.\frac{\partial^2\pi}{\partial z^2}\right|_{\mathrm{k1}} (h^* - h_{\mathrm{k1}})^2, \tag{7}$$

where k1 denotes the precomputed model-level index, h_{k1} is the height of the corresponding grid point, and h^* is the target height (the height of the velocity point). To avoid discretizing a second derivative, which can be rather inaccurate in the presence of a strong grid stretching, the second derivative is approximated using the hydrostatic equation $\partial\pi/\partial z = -g/c_{\mathrm{pd}}\theta_v$:

$$\pi^* = \pi_{\mathrm{k1}} + \left.\frac{\partial\pi}{\partial z}\right|_{\mathrm{k1}} (h^* - h_{\mathrm{k1}}) + \frac{1}{2}\frac{g}{c_{\mathrm{pd}}\theta_v^2}\left.\frac{\partial\theta_v}{\partial z}\right|_{\mathrm{k1}} (h^* - h_{\mathrm{k1}})^2. \tag{8}$$

It is mentioned that without the quadratic term, the Taylor-series approach becomes equivalent to the conventional discretization if the discretization stencil stays within one model layer (i.e., k1 is the same on both sides of a given velocity point) and the gradient is computed with centered second-order differences. The quadratic term then almost cancels out because $|h^* - h_{\mathrm{k1}}|$ is the same on both sides. Over steep topography, however, omitting the quadratic term turned out to increase the (spurious) winds in resting-atmosphere tests, particularly if a vertically stretched grid is used without a reference state.

A particularly tricky problem is the pressure-gradient computation on slope points, or more generally, on grid points for which the corresponding h^* is below the ground on one of the sides. Under such circumstances, the discretization in Eq. (8) involves the downward extrapolation of vertical gradients over distances that may be one to two orders of magnitude larger than the layer within which they have been evaluated. This degrades the accuracy of the discretization and potentially limits numerical stability, even though the stability threshold is usually higher than for the conventional discretization. To circumvent this extrapolation problem, Eq. (8) is applied only on those grid points for which h^* is not less than the maximum topography height of the adjacent mass points minus some tolerance value that is set to a default of 5 m in our implementation. Let k^* denote the lowest model level of a velocity gridpoint column for

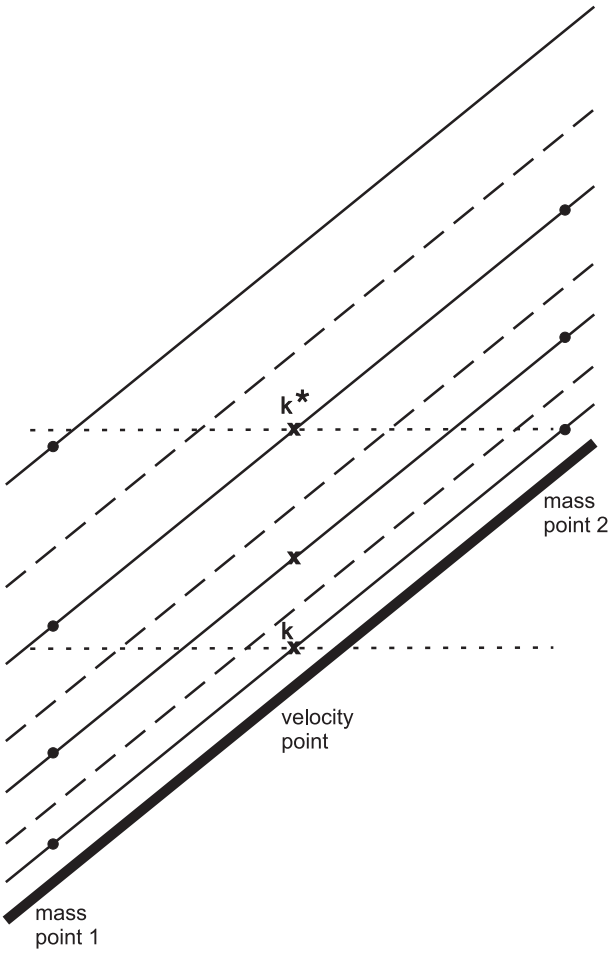

FIG. 1. Illustration of the discretization of the lower boundary condition according to Eq. (10). Solid (dashed) lines indicate main levels (layer interfaces). See text for further explanation.

which the pressure gradient can be computed from Eq. (8) without violating the extrapolation limit (see Fig. 1 for illustration). For any level k beneath k^*, we then use the relationship

$$\left.\frac{\partial \pi}{\partial n}\right|_{k} = \left.\frac{\partial \pi}{\partial n}\right|_{k^*} + \left.\frac{\partial^2 \pi}{\partial n \partial z}\right|_{k^*} (h_k - h_{k^*}), \tag{9}$$

or, using the same hydrostatic approximation as above,

$$\left.\frac{\partial \pi}{\partial n}\right|_{k} = \left.\frac{\partial \pi}{\partial n}\right|_{k^*} + \frac{g}{c_{\mathrm{pd}}\theta_v^2}\left.\frac{\partial \theta_v}{\partial n}\right|_{k^*} (h_k - h_{k^*}). \tag{10}$$

This way, extrapolating a vertical derivative of π is replaced by extrapolating a horizontal derivative of θ_v. It is mentioned that evaluating the $\partial\theta_v/\partial n$ term at level k^* rather than averaging it somehow over the extrapolation layer turned out to be beneficial in the case of an inversion intersecting a slope between the levels k^* and k, which is known to be prone to large discretization errors (e.g., Mesinger 1982; Janjić 1989). This can be understood by the fact that a horizontal (nonsloping) inversion layer, such as frequently occurring in weak-wind situations, does not alter the horizontal pressure gradient in reality. However, it almost inevitably causes errors in the discretization of the horizontal temperature gradient if this gradient is not evaluated in a truly horizontal manner (which is not possible below level k^*).

For completeness, we note the modifications required if a reference state is used, assuming that this reference state has already been implemented for the conventional discretization. We further assume that the reference state depends on height only and fulfills the hydrostatic balance condition analytically. Under these circumstances, the only term needing recalculation is the second derivative in Eq. (7), which is taken from the perturbation Exner function in this case. Let the subscript "0" and the prime denote reference and perturbation quantities, respectively. From

$$\begin{aligned}\frac{\partial}{\partial z}(\pi_0 + \pi') &= -\frac{g}{c_{\mathrm{pd}}(\theta_0 + \theta')} \\ &= -\frac{g}{c_{\mathrm{pd}}\theta_0}\left(1 - \frac{\theta'}{\theta_0} + \text{higher order terms}\right)\end{aligned} \tag{11}$$

follows, exploiting the hydrostatic balance of the reference state,

$$\frac{\partial \pi'}{\partial z} = -\frac{\theta'}{\theta_0}\frac{d\pi_0}{dz}, \tag{12}$$

which yields after differentiation

$$\frac{\partial^2 \pi'}{\partial z^2} = -\frac{\partial \theta'}{\partial z}\frac{1}{\theta_0}\frac{d\pi_0}{dz} - \theta'\frac{d}{dz}\left(\frac{1}{\theta_0}\frac{d\pi_0}{dz}\right). \tag{13}$$

To minimize the computational cost added by these modifications, a number of optimizations have been applied. First, the truly horizontal (Mahrer type) discretization with Taylor-series expansion [Eq. (8)] is applied only on those model levels where the precomputed k1 indices are not all identical to the level index of the corresponding velocity point. Thanks to the SLEVE coordinate, this typically restricts the more expensive algorithm to about the half of the model levels. Second, all indices, extrapolation distances and, if applicable, expressions involving the reference state, are precomputed and stored. Third, the special treatment of (near) slope points, Eq. (10), is handled via an index list. Within the ICON environment, we found an increase of the

computational cost of the dry dynamical core by about 2% for the global model or regional model domains including high mountain ranges.

For comparison, and inspired by the suggestions of the reviewers, linear, quadratic, and cubic polynomial interpolation have also been tested. As higher-order extrapolation to target points below the ground (not surprisingly) turned out to be numerically unstable for larger extrapolation distances, it was combined with the above-mentioned reformulation [Eq. (10)] for points lying more than 5 m below ground. Moreover, cubic interpolation was reduced to quadratic interpolation/extrapolation beneath the second model level from below. To briefly summarize, linear and quadratic interpolation turned out to yield somewhat larger discretization errors than the Taylor-series expansion method proposed above. Quadratic interpolation suffers from the problem that either the data points are not distributed symmetrically around the target point or the pressure reconstruction can become discontinuous at the level where the selection of the data points changes. Cubic interpolation was found to perform at least as well as our Taylor-series expansion method, but to be computationally a bit more expensive.

c. *Truly horizontal temperature diffusion*

For dynamical cores requiring an explicit numerical diffusion term on temperature for stability reasons, like for instance the leapfrog centered-difference scheme of the fifth-generation Pennsylvania State University–National Center for Atmospheric Research (PSU–NCAR) Mesoscale Model (MM5), Zängl (2002) showed that computing the diffusion on terrain-following coordinate surfaces (without a metric correction term) induces potentially large errors over mountainous terrain. To minimize these errors, he implemented a similar discretization as proposed by Mahrer (1984) for the pressure gradient. This approach will be referred to as truly horizontal diffusion in the following.

With upwind-biased advection discretizations for at least the scalar variables, such as used in ICON and many other ''modern'' numerical models, an artificial numerical filter with a flow-independent background diffusion coefficient is in principle not needed for stability reasons. A caveat, however, pertains to the numerical behavior over steep topography under weak or vanishing ambient flow. Under such conditions, a noisy small-scale flow with heavily distorted isentropes tends to develop (e.g., Zängl 2002; Zängl et al. 2004; Klemp 2011; see also Fig. 2), which can be greatly alleviated with a SLEVE coordinate or similar approaches (Klemp 2011) and suppressed, irrespective of the coordinate definition, with a truly horizontal temperature diffusion (Zängl 2002; Zängl et al. 2004). Thus, the decision has been made to implement such a feature into ICON as well, but with two essential differences to the above-mentioned MM5 implementation. First, a second-order diffusion operator is used in ICON (as opposed to fourth-order in MM5) because this allows combining it with the Smagorinsky diffusion implemented to parameterize horizontal mixing under strong flow deformation. Second, the truly horizontal diffusion is applied only on grid points exceeding a certain slope threshold (see below for details). It is mentioned that the potential alternative, a second-order diffusion operator with full metric correction terms (evaluated along the terrain-following coordinate surfaces), has been discarded because of the stability restrictions on the diffusion coefficient over steep slopes. Recall that with an explicit time-stepping scheme, including the metric terms reduces the Courant–Friedrichs–Lewy (CFL) stability limit on the diffusion coefficient by a factor of $(\Delta h/\Delta z)^2$, with Δh denoting the height difference between two neighboring grid points and Δz denoting the layer thickness.

In the ICON implementation, the truly horizontal θ_v diffusion is applied only on grid points on which either the maximum height difference to one of the neighboring grid points or the related slope exceeds a certain threshold value. The default values, which are used in the test experiments presented below, are $\Delta h_{\text{th}} = 200$ m for the height difference and $\alpha_{\text{th}} = 0.02$ for the slope α. The motivation for this (empirically determined) combined criterion is due to the fact that at horizontal mesh sizes typically used for global modeling, the height difference is the limiting factor for numerical stability and the magnitude of discretization errors, whereas the slope takes over at finer resolutions. On global model domains, the fraction of model grid points fulfilling the above criteria is typically on the order of 1%, with some variability depending on the coordinate setup and the amount of topography filtering. The truly horizontal diffusion has therefore been implemented via an index list acting only on those grid points where the diffusion is actually applied. This way, the computational overhead is usually negligible.

If the truly horizontal diffusion is applied in combination with a Smagorinsky diffusion for θ_v, the Smagorinsky diffusion tendency is first computed on all grid points along terrain-following coordinate surfaces (without metric correction terms for the reason mentioned above). Then, it is overwritten with the truly horizontally computed value on the grid points included in the index list, using the same flow-dependent diffusion coefficient as in the first step. In addition, a background diffusion coefficient K_{bg} is specified for the truly horizontal diffusion because it is needed to suppress the numerical noise in atmosphere-at-rest tests. It is formulated as

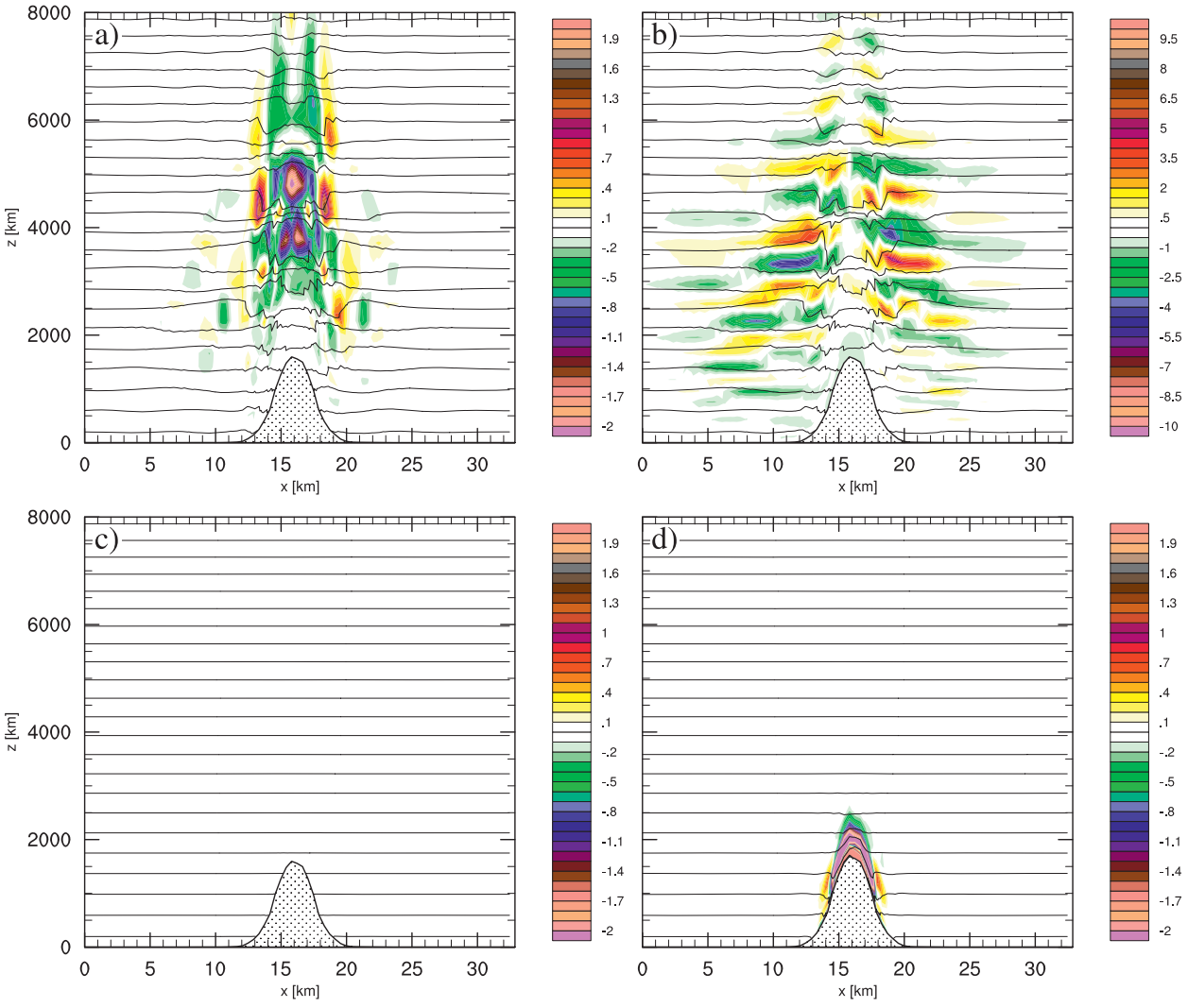

FIG. 2. Results at $t = 6$ h for atmosphere-at-rest experiments with conventional pressure-gradient discretization; $h_m = 1750$ m without truly horizontal temperature diffusion, solid lines denote potential temperature (contour interval 4 K), color shading indicates (a) vertical wind speed and (b) horizontal wind speed (m s^{-1}). (c) As in (a), but with truly horizontal temperature diffusion. (d) As in (a), but $h_m = 1850$ m with truly horizontal temperature diffusion. Note that the mountain height appearing in the graphs is somewhat less than the nominal h_m value because of the horizontal remapping required for plotting vertical cross sections.

a nondimensional diffusion coefficient per time step in the following way:

$$K_{\mathrm{bg}} = \mathrm{MAX}\left(4\times10^{-3}\sqrt{\alpha-\alpha_{\mathrm{th}}}, 2\times10^{-4}\sqrt{\Delta h-\Delta h_{\mathrm{th}}}\right);$$
$$K_{\mathrm{bg}} = \mathrm{MIN}(5\times10^{-3},\ K_{\mathrm{bg}}). \qquad (14)$$

We note in addition that while a conservative formulation as $\nabla\cdot(K_h\nabla\theta)$ is straightforward to implement for the conventional Smagorinsky diffusion along terrain-following coordinates, a conservative discretization is not possible for the truly horizontal diffusion. For simplicity, the truly horizontal diffusion is therefore formulated as $K_h\nabla^2\theta$. Here, priority has been given to the minimization of local errors at the expense of global conservation properties. In addition, the truly horizontal diffusion is not applied at slope points, or more precisely, at all grid points where the truly horizontal stencil would lie below the lowest main model level at one of the neighbor points. This way, detrimental effects on the formation of slope wind circulations are avoided [see Zängl (2002) for a more detailed discussion of this aspect].

3. Tests and results

a. *Isolated steep mountain*

To assess the benefits and limitations of the developments described above, several series of tests at

varying levels of idealization have been conducted. Our first, most highly idealized, test series considers an isolated circular Gaussian mountain in an isothermal, horizontally homogeneous, hydrostatically balanced atmosphere at rest. For the experiments presented in the following, the *e*-folding width of the mountain is 2000 m and the horizontal resolution of the model grid is about 300 m. It is pointed out that the grid used here is based on the icosahedral triangulation of the sphere (as it has to be done for global simulations), which implies that the grid is not regular and has no symmetry with respect to the mountain peak. The magnitude of the numerical disturbances may therefore be larger than for a regular (planar) grid that exploits the possible symmetry conditions. In the vertical, the model grid has 50 main levels with a top at 40 km. For the experiments shown below, the lowest level is located at 10 m above ground, which is the standard for applications in numerical weather prediction (NWP). However, sensitivity tests with other settings have also been conducted and will be mentioned in the discussion where appropriate. The only physics parameterization used for the idealized-mountain tests is a turbulent vertical mixing scheme that includes a background (flow independent) vertical diffusion of 0.1 $m^2\ s^{-1}$ on momentum and temperature. The reference atmosphere temperature profile is given by

$$T_0(z) = T_{\rm str} + (T_{\rm sl} - T_{\rm str}) \exp\left(-\frac{z}{H_{\rm scal}}\right), \quad (15)$$

where $T_{\rm sl} = 288.15$ K, $T_{\rm str} = 213.15$ K, and $H_{\rm scal} = 10\ 000$ m. The low-level vertical temperature gradient of the reference atmosphere thus differs strongly from the isothermal atmosphere specified as initial condition, implying that the use of the reference atmosphere has only little impact on the magnitude of the discretization errors.

Selected results obtained after 6 h of integration with the conventional pressure gradient discretization are displayed in Fig. 2. The maximum mountain height h_m is 1750 m in Figs. 2a–c and 1850 m in Fig. 2d, corresponding to a maximum slope of 0.74 and 0.78, respectively. Without the truly horizontal temperature diffusion scheme described above, a noisy flow pattern with strongly distorted isentropes and substantial horizontal and vertical wind speeds develops during the first hour of integration and has reached a quasi-steady state by $t =$ 6 h (Figs. 2a,b). The flow pattern is characterized by alternating inflow and outflow in the horizontal and mostly subsiding flow right above the mountain peak. It does not depend qualitatively on the use of a vertical mixing scheme (not shown). Note that the lack of symmetry with respect to the mountain peak is due to the above-mentioned irregularity of the model grid. With truly horizontal temperature diffusion, the disturbances are suppressed almost completely (Fig. 2c). For all experiments discussed in the remainder of this paper, the truly horizontal diffusion scheme is used as well because this facilitates highlighting the direct effects of the pressure-gradient discretization.

Increasing h_m from 1750 to 1850 m triggers a different type of spurious flow that is mostly confined to the near-surface model levels above the upper half of the mountain (Fig. 2d). This flow pattern is the manifestation of a numerical instability that causes the model to blow up within the first hour of integration for mountain heights of 2000 m or more. The onset of this numerical instability depends sensitively on the thickness of the lowest model layer. For example, with the lowest main level located at 25 m above ground, a qualitatively similar flow pattern as shown in Fig. 2d appears for $h_m =$ 3000 m, and the instability starts at a height of about 3200 m (not shown). This indicates that the ratio $\Delta h/\Delta z$ is an important factor affecting this instability, but tests at coarser horizontal resolutions revealed that the slope itself plays a role as well, with the $\Delta h/\Delta z$ threshold getting larger at coarser resolutions.

With the truly horizontal pressure-gradient discretization, including the reformulated lower boundary condition described in Eq. (10), the model atmosphere remains nearly at rest up to a mountain height of about 4000 m (Fig. 3a). The maximum slope in this case is 1.7, or about 60°. With further increasing mountain height, the magnitude of the spurious circulation developing over the upper half of the mountain gradually grows, but even for $h_m = 7000$ m (Fig. 3b), it is not as large as with the conventional discretization and $h_m = 1850$ m (Fig. 2d). Additional experiments indicated that the magnitude of the spurious circulations depends only weakly on the near-surface vertical resolution. Moreover, the numerical stability limit is rather insensitive against the details of the model layer setup, typically ranging between mountain heights of 7200 and 7500 m. Turning off the truly horizontal temperature diffusion does not significantly affect numerical stability either, even though the isentropes above the mountain become distorted in a similar way as shown in Figs. 2a,b. However, turning off the vertical mixing scheme has a substantial detrimental impact for mountain heights exceeding about 4000 m and reduces the stability limit to about 6000 m. When omitting the improved lower boundary condition [Eq. (10)], the stability limit even decreases to mountain heights of about 4000 m. Below this value, the magnitude of the circulations is then several times larger than with the full scheme at the lowest model level, but the differences at higher levels are relatively small (not

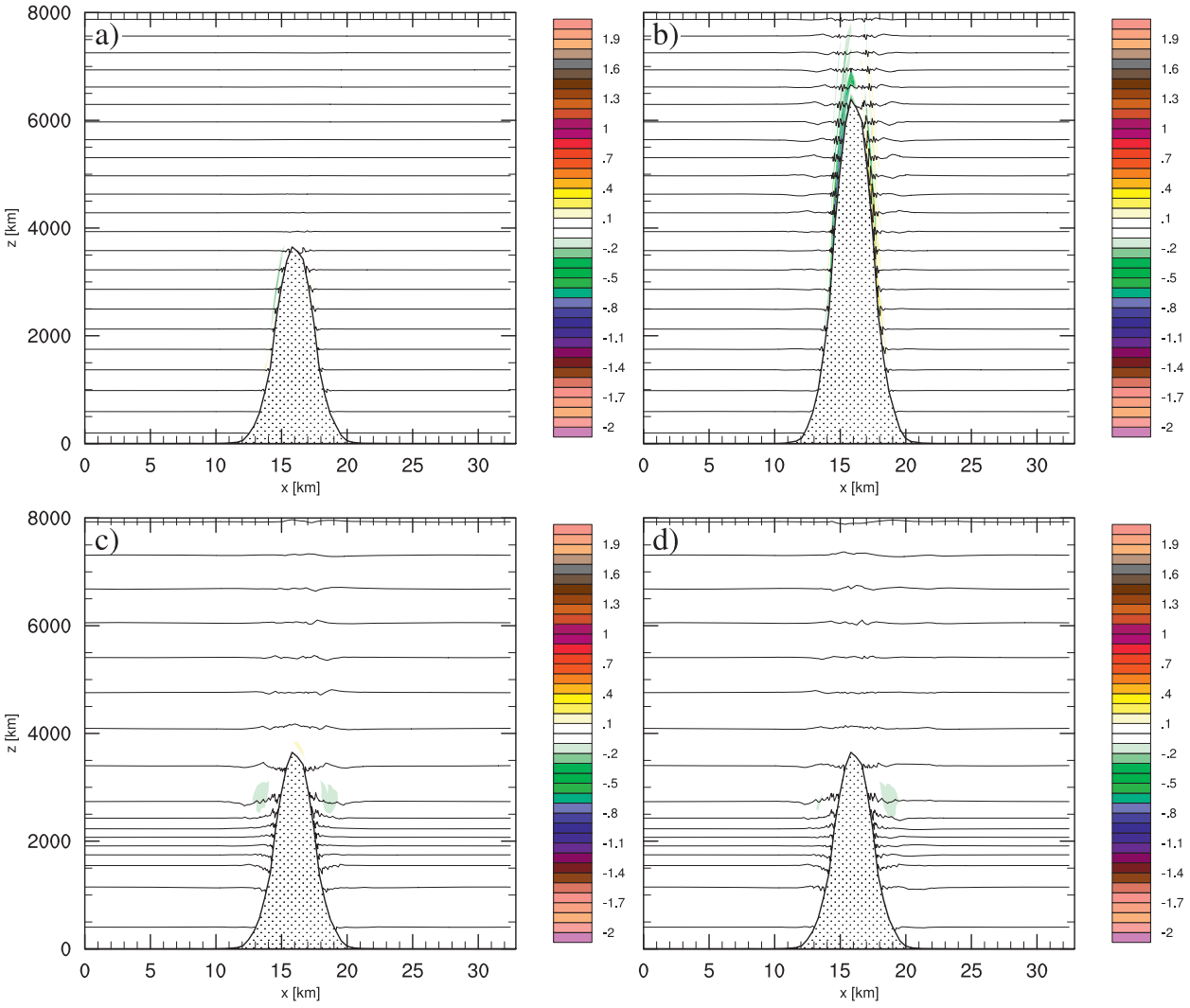

FIG. 3. Results at $t = 6$ h for atmosphere-at-rest experiments with truly horizontal pressure gradient discretization and truly horizontal temperature diffusion: (a) $h_m = 4000$ m, isothermal atmosphere; (b) $h_m = 7000$ m, isothermal atmosphere; and (c) $h_m = 4000$ m, multilayer atmosphere. (d) As in (c), but Taylor-expansion-based pressure reconstruction is replaced with cubic interpolation. Solid lines denote potential temperature [the contour interval is 4 K in (a),(b) and 2 K in (c),(d)], and color shading indicates vertical wind speed (m s^{-1}).

shown). Results for sensitivity experiments with a more complex temperature profile are displayed in Figs. 3c,d. In this setup, the Brunt–Väisälä frequency N is set to 0.02 s^{-1} between 1500 and 2500 m and above 12 000 m, and to 0.01 s^{-1} elsewhere. Here h_m is 4000 m as in Fig. 3a. Comparing Fig. 3c with Fig. 3a reveals that the localized inversion leads to a somewhat stronger distortion of the isentropes, even though the wind speeds appearing in the graphs are not significantly larger. The distortion now extends above the mountain peak, and there is a tendency for the inversion to be smeared out where it intersects the mountain slope. The corresponding result for cubic interpolation (Fig. 3d) indicates almost no improvement over the Taylor-expansion-based method used otherwise. A more detailed inspection of the model output revealed that the spurious circulations grow more slowly in the initial simulation phase with cubic interpolation, but saturate at a comparable level after some hours of simulation. A similar behavior was observed for several other cases tested.

To inspect the model behavior in more complex orography, the so-called Schär mountain proposed by Schär et al. (2002),

$$h(x) = h_m \exp\left[-\left(\frac{x}{a}\right)^2\right] \cos\left(\frac{\pi x}{\lambda}\right)^2, \tag{16}$$

has been considered in addition. Our first example serves for comparison with Fig. 1 of Klemp (2011), using $h_m = 1000$ m, $a = 5000$ m, and $\lambda = 4000$ m. The decay

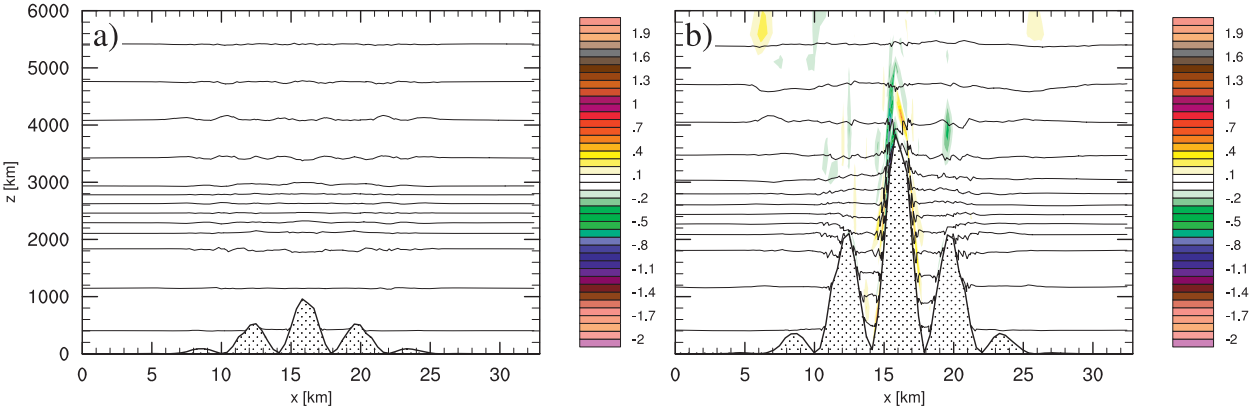

FIG. 4. Results at $t = 6$ h for atmosphere-at-rest experiments with multilayer atmosphere and Schär mountain with (a) $h_m = 1000$ m and (b) $h_m = 4000$ m. Solid lines denote potential temperature (the contour interval is 4 K) and color shading indicates vertical wind speed (m s^{-1}).

parameters of the SLEVE coordinate have been chosen to be as close as possible to Fig. 1g of Klemp (2011), taking into account that the algorithm used to generate the filtered (large scale) topography differs because of restrictions related to our unstructured triangular grid. Moreover, because of the lack of a two-dimensional slice model version, a quasi-2D ridge with constant height over 20 km in the y direction is used, and it is noted again that there is no symmetry of the model grid with respect to the orography. The result for the truly horizontal pressure-gradient scheme is shown in Fig. 4a. Similar to the corresponding result (Fig. 1h) of Klemp (2011), there is only a minor distortion of the isentropes visible above the mountain. Because of the rapid decay of the topography signal in the coordinate surfaces present in this configuration, the results are almost as good with the conventional pressure-gradient discretization and without the truly horizontal diffusion scheme (not shown). A significantly more demanding setup arises by increasing h_m to 4000 m, corresponding to a maximum slope of about 2.7 (70°; Fig. 4b). In this case, the inversion again intersects the mountain and gets diffused vertically, leading to enhanced static stability in the valleys between the primary ridge and the secondary ridges. Moreover, the distortion of the isentropes above the mountain peaks is now more notable. Nevertheless, the numerical errors are not so large that real-case simulations considering comparably steep orography would have to be regarded a priori as useless.

Results from another set of experiments with a constant wind speed of $U = 20$ m s^{-1}, and again an isothermal atmosphere and a circular Gaussian mountain are shown in Fig. 5. The two top panels compare the results of the conventional pressure-gradient discretization with those of the truly horizontal scheme for a mountain height of 1750 m, for which the conventional discretization is still numerically stable. In this case, the gravity wave pattern developing above and in the lee of the mountain is practically indistinguishable for the two schemes. This is not too surprising as both discretizations are second-order accurate. It is pointed out that a strong leeward component of the group velocity has to be expected for the setup chosen here, as the nondimensional mountain width Na/U, where $a \approx 1665$ m is the mountain half-width, is about 1.5 (see, e.g., Queney 1948). With further increasing mountain height, the gravity wave activity over the mountain decreases because the flow regime more and more changes from a flow over the mountain to a flow around the mountain. This is again in line with the existing knowledge about flow over mountains as the nondimensional mountain height Nh_m/U is already about 1.6 for $h_m = 1750$ m. Moreover, a recirculating wake with turbulent eddies forms at low levels in the lee of the mountain. For $h_m = 4000$ m (Fig. 5c), there are only weak vertically oriented flow features visible above the mountain peak that could be categorized as questionable based on common knowledge about gravity wave dynamics (a more quantitative statement is difficult because the mesoscale models available to the author are not numerically stable for this mountain height). A more unusual flow pattern appears for $h_m = 7000$ m (Fig. 5d), where a narrow, line-shaped zone of upward motion extends from the upper windward slope nearly vertically upward. This feature turned out to be quite robust against changes of the static stability and (moderate) reductions of the mountain height, indicating that it is not related to an upcoming numerical instability. However, addressing the question if this is an artifact or not must be postponed until a later investigation.

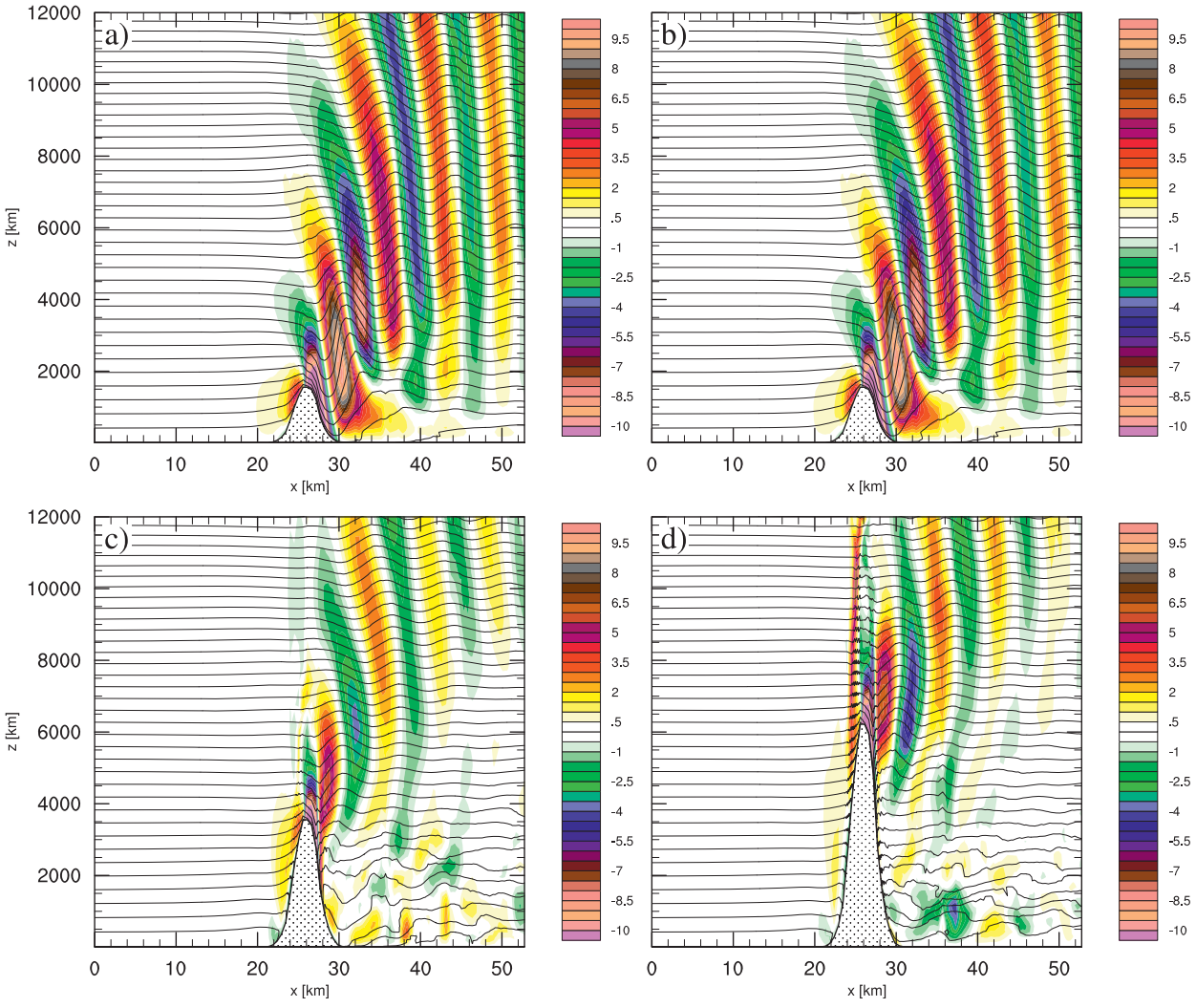

FIG. 5. Results at $t = 6$ h for experiments with isothermal atmosphere and $U = 20$ m s^{-1}: (a) $h_m = 1750$ m, conventional pressure-gradient discretization; (b) $h_m = 1750$ m, truly horizontal pressure-gradient discretization; (c) as in (b), but $h_m = 4000$ m; and (d) as in (b), but $h_m = 7000$ m. Solid lines denote potential temperature (contour interval 4 K) and color shading indicates vertical wind speed (m s^{-1}).

b. Global model with real orography

As one primary goal of the ICON development at DWD is global numerical weather prediction, it is clear that a huge number of global simulations with real topography, real initial data, and full physics coupling have already been conducted. So far, the most extensive test series have been performed for horizontal mesh sizes of 40 and 20 km, with integration periods of 30 and 7 days, respectively. Using 30″ topography data as input to our external parameter software, and turning off topography filtering completely, the maximum height difference between adjacent model grid points is then about 2840 and 2410 m, respectively. Under these conditions, the model usually blows up within single-digit number of time steps with the conventional pressure-gradient discretization. With the truly horizontal scheme without the improved lower boundary condition [Eq. (10)], the model still tends to blow up within less than 20 time steps, even though the minimum amount of topography smoothing required for numerical stability is less than for the conventional discretization. On the other hand, the ICON model usually runs numerically stable over the full integration period with the truly horizontal scheme including Eq. (10), even without any topography smoothing. This indicates that the pressure-gradient discretization proposed in this work is beneficial for a wide range of spatial resolutions, covering two orders of magnitude from mesh sizes relevant for global modeling down to the transition zone toward large-eddy simulations.

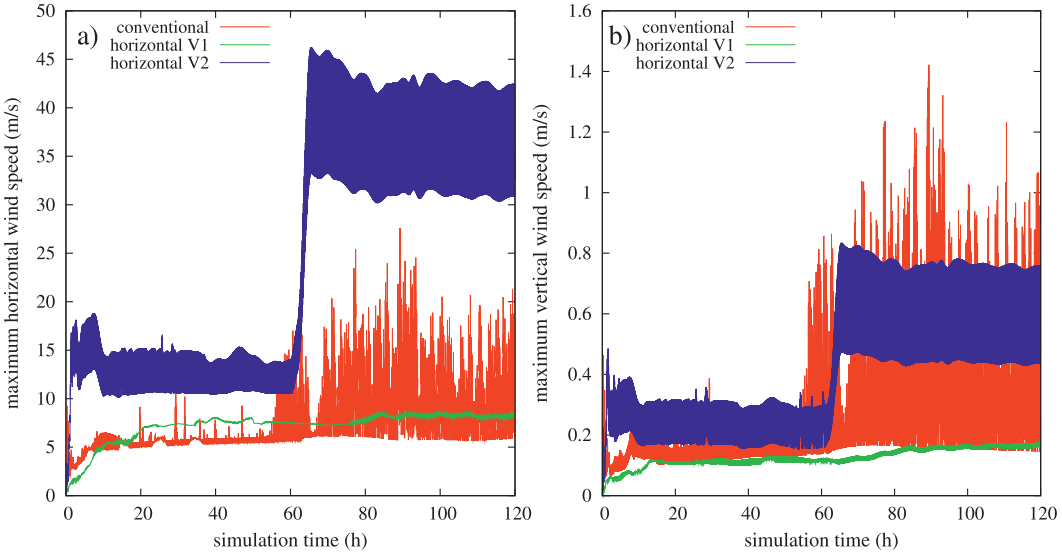

FIG. 6. Time series of domain-wide maximum (a) horizontal and (b) vertical wind speed (m s^{-1}) for global simulation (mesh size is 40 km) initialized with an isothermal atmosphere at rest. Because data are plotted at every sound wave time step (68 s), high-frequency fluctuations may therefore appear as solid coloring. "Horizontal V1" ("horizontal V2") denotes the full (simplified) truly horizontal pressure-gradient discretization.

Besides the question if a model runs numerically stable at all, the magnitude of the spurious circulations induced over the grand mountain ranges on the earth (Andes, Himalayas) is of significant interest. This issue has been addressed with semi-idealized simulations, combining real topography with an isothermal atmosphere at rest such as used for part of the highly idealized tests above. For the experiments discussed in the following, a horizontal mesh size of 40 km (327 680 mass points) has been combined with 90 model levels up to a top height of 67.5 km. The lowest main level is again at 10 m above ground. The model topography has been filtered as much as required to obtain numerically stable simulations over a period of 5 days for all options of the pressure-gradient discretization. Again, a turbulent vertical mixing scheme is the only physics parameterization applied. Time series of the maximum horizontal and vertical wind speed occurring anywhere in the model domain are displayed in Fig. 6. The conventional pressure-gradient discretization (red lines) is found to behave reasonably well during the first two days of the integration but then starts to develop substantial high-frequency oscillations with maximum horizontal speeds in excess of 20 m s^{-1}. Even stronger high-frequency oscillations are found for the truly horizontal discretization without the special lower boundary condition (blue lines). Moreover, a sudden jump to maximum horizontal wind speeds above 40 m s^{-1} occurs after about 60 h of simulation for this option. Even though these extreme values are confined to a few grid points and the lowest model layer (not shown), such a behavior would not be acceptable for operational applications. The overall best results are obtained with the complete truly horizontal scheme including Eq. (10) (green lines), which exhibits the lowest vertical wind speeds, the weakest high-frequency oscillations, and the slowest growth of the disturbances during the first 6 h. Only the maximum horizontal wind speeds are somewhat higher than for the conventional discretization during part of the integration period.

4. Summary and conclusions

To improve the numerical stability over steep mountain ranges, a truly horizontal pressure-gradient discretization inspired by the ideas of Mahrer (1984) has been developed and implemented into the ICON model. To reconstruct the pressure at the required auxiliary points, a second-order Taylor-series expansion is used. To reduce the discretization errors near the surface and/or in the presence of strong vertical grid stretching, the second derivative is transformed into a first derivative using the hydrostatic approximation. In addition, a special lower boundary condition has been developed that replaces the extrapolation of a vertical derivative of Exner pressure by the extrapolation of a horizontal derivative of potential temperature, which improves numerical stability if the height difference between adjacent grid points is much larger than the low-level vertical resolution. The truly horizontal pressure-gradient discretization is combined with a truly horizontal

temperature diffusion that suppresses the development of numerical noise in atmosphere-at-rest tests over steep mountains and thus helps isolating numerical problems directly related to the pressure-gradient discretization.

A sequence of tests with varying degree of idealization has been conducted to assess the benefits and limitations of the truly horizontal pressure-gradient discretization. Most importantly, the tests revealed a substantial improvement of numerical stability over steep slopes. This has been verified for a wide spectrum of horizontal resolutions, ranging from mesh sizes of a few hundreds of meters to mesh sizes of several tens of kilometers. At a mesh size of 300 m, our tests indicated trustable results up to slope angles of at least 60°, if not even 70°, both for atmosphere-at-rest tests and for simulations of airflow over a mountain. This limit depends only weakly on the vertical layer spacing near the surface, whereas the numerical stability limit for the conventional pressure-gradient discretization depends very sensitively on this parameter. With the lowest main level at 10 m above ground, which is the standard setting in NWP applications, the stability threshold of the conventional discretization has been found to be less than one-third of that of the truly horizontal discretization. At mesh sizes typical for global weather forecasting, this factor is not as large, but our results still indicate a substantial improvement. Using the reformulated lower boundary condition, Eq. (10), has been found to be much more important at coarse resolutions than at fine resolutions. One may therefore speculate that earlier attempts to implement a Mahrer-type pressure-gradient discretization in nonhydrostatic models were regarded as unsuccessful because of deficiencies at the lower boundary and thus never found their way into officially distributed model versions.

This leads us to the final discussion point about the portability of the discretization method presented here to other nonhydrostatic models. In general, a truly horizontal pressure-gradient discretization can be implemented for any set of prognostic thermodynamic variables (e.g., pressure–temperature, or perturbations of these quantities), but there is one potential advantage for equation systems using the Exner function for the calculation of pressure gradients. It appears because the hydrostatic approximation applied in Eqs. (8) and (10) to convert second derivatives into first derivatives—which are more convenient to discretize—leads to a larger number of individual terms in a pressure-temperature equation system than in our case. The ensuing increase of computing costs is probably a relatively unimportant disadvantage, but one could imagine situations in which cancellation effects between the individual terms increase the discretization errors. Whether this actually happens is difficult to determine without a detailed investigation, which is beyond the scope of this work, but given the large improvements of numerical stability that can be gained from a truly horizontal pressure-gradient discretization, our conclusion would be that it is definitely worth trying.

Acknowledgments. The author wants to thank all members of the ICON development team for their excellent work, without which the study presented here would not have been possible. Moreover, the constructive and insightful comments of the two anonymous reviewers are greatly appreciated, having led to further improvement of the manuscript.

REFERENCES

Dempsey, D., and C. Davis, 1998: Error analyses and tests of pressure-gradient force schemes in a nonhydrostatic mesoscale model. Preprints, *12th Conf. on Numerical Weather Prediction,* Phoenix, AZ, Amer. Meteor. Soc., 236–239.

Dudhia, J., 1995: Reply. *Mon. Wea. Rev.,* **123,** 2573–2576.

Gallus, W. A., and J. B. Klemp, 2000: Behavior of flow over step orography. *Mon. Wea. Rev.,* **128,** 1153–1164.

Gary, J. M., 1973: Estimate of truncation error in transformed coordinate, primitive equation atmospheric models. *J. Atmos. Sci.,* **30,** 223–233.

Janjić, Z. I., 1989: On the pressure gradient force error in σ-coordinate spectral models. *Mon. Wea. Rev.,* **117,** 2285–2292.

Klemp, J. B., 2011: A terrain-following coordinate with smoothed coordinate surfaces. *Mon. Wea. Rev.,* **139,** 2163–2169.

Leuenberger, D., M. Koller, O. Fuhrer, and C. Schär, 2010: A generalization of the SLEVE vertical coordinate. *Mon. Wea. Rev.,* **138,** 3683–3689.

Mahrer, Y., 1984: An improved numerical approximation of the horizontal gradients in a terrain-following coordinate system. *Mon. Wea. Rev.,* **112,** 918–922.

Mesinger, F., 1982: On the convergence and error problems of the calculation of the pressure gradient force in sigma coordinate models. *Geophys. Astrophys. Fluid Dyn.,* **19,** 105–117.

Miura, H., 2007: An upwind-biased conservative advection scheme for spherical hexagonal–pentagonal grids. *Mon. Wea. Rev.,* **135,** 4038–4044.

Queney, P., 1948: The problem of airflow over mountains: A summary of theoretical studies. *Bull. Amer. Meteor. Soc.,* **29,** 16–26.

Schär, C., D. Leuenberger, O. Fuhrer, D. Lüthi, and C. Girard, 2002: A new terrain-following vertical coordinate for atmospheric prediction models. *Mon. Wea. Rev.,* **130,** 2459–2480.

Steppeler, J., H.-W. Bitzer, M. Minotte, and L. Bonaventura, 2002: Nonhydrostatic atmospheric modeling using a z-coordinate representation. *Mon. Wea. Rev.,* **130,** 2143–2149.

Zängl, G., 2002: An improved method for computing horizontal diffusion in a sigma-coordinate model and its application to simulations over mountainous topography. *Mon. Wea. Rev.,* **130,** 1423–1432.

——, 2003: A generalized sigma coordinate system for the MM5. *Mon. Wea. Rev.,* **131,** 2875–2884.

——, L. Gantner, G. Hartjenstein, and H. Noppel, 2004: Numerical errors above steep topography: A model intercomparison. *Meteor. Z.,* **13,** 69–76.